AJNR

Dynamic Contrast-enhanced T2*-weighted MR Imaging of Tumefactive Demyelinating Lesions

Soonmee Cha, Sean Pierce, Edmond A. Knopp, Glyn Johnson, Clement Yang, Anthony Ton, Andrew W. Litt and David Zagzag

AJNR Am J Neuroradiol 2001, 22 (6) 1109-1116
http://www.ajnr.org/content/22/6/1109

AJNR Am J Neuroradiol 22:1109–1116, June/July 2001

Dynamic Contrast-enhanced T2*-weighted MR Imaging of Tumefactive Demyelinating Lesions

Soonmee Cha, Sean Pierce, Edmond A. Knopp, Glyn Johnson, Clement Yang, Anthony Ton, Andrew W. Litt, and David Zagzag

***PURPOSE*: Dynamic contrast-enhanced T2*-weighted MR imaging has been helpful in characterizing intracranial mass lesions by providing information on vascularity. Tumefactive demyelinating lesions (TDLs) can mimic intracranial neoplasms on conventional MR images, can be difficult to diagnose, and often result in surgical biopsy for suspected tumor. The purpose of this study was to determine whether dynamic contrast-enhanced T2*-weighted MR imaging can be used to distinguish between TDLs and intracranial neoplasms that share common features on conventional MR images.**

***METHODS*: We retrospectively reviewed the conventional and dynamic contrast-enhanced T2*-weighted MR images and medical records of 10 patients with tumefactive demyelinating disease that was diagnosed by either biopsy or strong clinical suspicion supported by laboratory evaluation that included CSF analysis and evoked potential tests. Twelve TDLs in 10 patients and 11 brain tumors that appeared similar on conventional MR images were studied. Relative cerebral blood volume (rCBV) was calculated from dynamic MR data and was expressed as a ratio to contralateral normal white matter. rCBV values from 11 patients with intracranial neoplasms with very similar conventional MR imaging features were used for comparison.**

***RESULTS*: The rCBV values of TDLs ranged from 0.22 to 1.79 (n = 12), with a mean of 0.88 ± 0.46 (SD). The rCBV values of intracranial neoplasms ranged from 1.55 to 19.20 (n = 11), with a mean of 6.47 ± 6.52. The difference in rCBV values between the two groups was statistically significant ($P = .009$). The difference in rCBV values between TDLs and primary cerebral lymphomas (n = 4) was less pronounced but was statistically significant ($P = .005$).**

***CONCLUSION*: Dynamic contrast-enhanced T2*-weighted MR imaging is a useful diagnostic tool in differentiating TDLs from intracranial neoplasms and may therefore obviate unnecessary surgical biopsy.**

Tumefactive demyelinating lesions (TDLs) can mimic intracranial neoplasms and pose a diagnostic dilemma, both with clinical presentation and conventional MR imaging features. On images, TDLs and high-grade intracranial neoplasms can both show contrast enhancement, perilesional edema, varying degrees of mass effect, and central necrosis (1–3). Furthermore, TDLs can be confused with high-grade glial neoplasms on histopathologic evaluation because of the presence of hypercellularity and atypical reactive astrocytes with mitotic figures (1). Single dominant TDLs, in particular, are often misdiagnosed as brain tumors, leading to unnecessary, and possibly harmful, biopsy or even resection. In some instances, patients with TDLs were subjected not only to surgery but also to radiation therapy for a mistaken diagnosis of lymphoma or glioma (1, 2). Considering this diagnostic dilemma, there are several reports in the pathology literature that have stressed the need for special stains for myelin and axons to make the correct diagnosis of TDLs (1, 4–6). Numerous radiologic reports also have addressed TDLs masquerading as brain tumors and leading to unnecessary surgery (2, 3, 6, 7).

One of the key histopathologic differences between TDLs and high-grade brain tumors is the absence of frank angiogenesis of the former. The blood vessels within areas of demyelination are intrinsically normal without evidence of neovascu-

Received July 25, 2000; accepted after revision November 17.

From the Departments of Radiology (S.C., S.P., E.A.K., G.J., C.Y., A.T., A.W.L.), Neurosurgery (E.A.K., D.Z.), and Pathology (D.Z.), Division of Neuropathology, and the Kaplan Cancer Center (E.A.K., D.Z.), New York University Medical Center, New York, NY.

This work was presented in part at the Annual Meeting of the American Society of Neuroradiology, April 2000, Atlanta, GA, and received the Outstanding Presentation Award in the General Neuroradiology category.

Address reprint requests to Soonmee Cha, MD, 530 First Avenue, New York University Medical Center, HCC-Basement, MRI Center, New York, NY 10016.

larization (1, 4). In contrast, tumor angiogenesis is one of the characteristic hallmarks of high-grade brain tumors (8–11). The purpose of our study, therefore, was to determine whether MR measurements of cerebral blood volume could be used to differentiate between TDLs and intracranial neoplasms. We herein report that by assessing lesion vascularity, dynamic contrast-enhanced T2*-weighted MR imaging can be valuable in differentiating TDLs and intracranial neoplasms that share similar conventional MR imaging features.

Methods

At our institution, all patients with suspected brain tumors undergo dynamic, contrast-enhanced T2*-weighted MR imaging to obtain measurements of relative cerebral blood volume (rCBV). Approval for these studies was obtained from the Institutional Board of Research Associates, and informed consent was obtained from all patients.

During the last 3 years, a total of 10 patients with suspected brain tumors were diagnosed as having TDLs by either biopsy or strong clinical suspicion supported by laboratory examinations that included CSF analysis and/or somatosensory evoked potential tests. Although there are a variety of criteria for the diagnosis of TDLs, the main criterion was clinical follow-up with a presumed, but not documented, regression of the lesions. There were eight patients with one lesion each, one patient with two lesions, and one patient with three lesions. Patient age ranged from 13 to 57 years, with a mean age of 34.5 years; seven were female and three were male patients. Clinically, the patients had acute or subacute clinical onset of symptoms and signs of either focal neurologic deficit or increased intracranial pressure mimicking those of an intracranial neoplasm. One patient was found to be HIV-positive but without any systemic manifestation of AIDS. The remaining patients did not have any systemic illness or malignancy or evidence of immunosuppression.

For comparison, 11 patients with intracranial neoplasms (six high-grade gliomas, one low-grade glioma, and four lymphomas) that showed very similar conventional MR imaging features (eg, minimal edema and mass effect, well-circumscribed border, definite but varying degrees of contrast enhancement, and predominantly located within white matter) were chosen. Patients with intracranial neoplasms that had classic MR imaging features of high-grade gliomas (eg, extensive edema with mass effect, irregular enhancement and infiltrative pattern, and presence of extensive necrosis) and typical features of primary cerebral lymphomas (eg, multiple deep gray matter lesions and subependymal spread) were excluded. Patient age ranged from 28 to 84 years, with a mean of 52 years; four were female and seven were male patients.

Before imaging, a 20- or 22-gauge IV catheter was inserted in the antecubital area for contrast agent administration. Imaging was performed on a 1.5-T scanner. Localizing sagittal T1-weighted images were obtained, and then axial T1-weighted (600/14/1 [TR/effective TE/excitation]), T2-weighted (3400/119/1), and axial fluid-attenuated inversion recovery (9000/110/1; inversion time, 2200 ms) images of the brain were obtained. The location and size of the lesion and the position of the superior and inferior margins were determined from the T2-weighted and fluid-attenuated inversion recovery images. A series of T2*-weighted gradient-echo echo-planar images (1000/54/1) was then acquired during the first pass of a bolus of contrast agent. Five to seven sections, 3 to 5 mm thick (gap, 0–20%), were selected to cover the entire lesion volume. The first 10 image sets were obtained before the injection of contrast agent to establish an unenhanced baseline. At the 10th acquisition, contrast agent (0.1 mmol/kg) was injected by power injector at a rate of 3 or 5 mL/s (total volume of 18 mL) through the antecubital angiocatheter; 20 mL of continuous saline flush was then immediately administered. Finally, contrast-enhanced axial T1-weighted images were obtained.

The raw T2*-weighted echo-planar images were transferred to an UltraSPARC station (Sun Computer, Mountain View, CA) for processing. All software programs for postprocessing were developed in house using the C and IDL programming languages (Research Systems, Inc., Boulder, CO). Details of data processing are fully described by Knopp et al (12), and only a summary is included herein. During the first pass of the paramagnetic contrast bolus, signal intensity drops on T2*-weighted images. The concentration of contrast agent can be calculated from signal intensity changes to obtain a plot of tissue contrast agent concentration over time. The area under this curve is proportional to the regional cerebral blood volume. Correction for contrast recirculation and leakage (which invalidates the cerebral blood volume calculation) was performed by subtracting a baseline from under the contrast bolus. The beginning and end of the bolus were defined as the images at which the signal came within 1 SD of the mean pre- and post-bolus signals, respectively. The baseline drawn between these two points was then subtracted from the signal.

The constant of proportionality is unknown in these calculations, so that cerebral blood volume must be expressed relative to an internal reference, such as the normal contralateral white matter and these values are the rCBV values. Color overlay maps of both rCBV and maximum signal drop were formed (13). To improve signal-to-noise ratio in the measurements, rCBV values were then calculated in regions of interest in areas showing the greatest values on the maps.

Conventional MR images were analyzed for lesion size, number and location of lesions, degree of contrast enhancement, perilesional edema, presence or absence of necrosis, and mass effect. In the patient with three lesions, the most inferior lesion was at a large distance from the other two and was excluded from the dynamic contrast-enhanced study. At least five rCBV measurements were obtained in different regions of interest within the lesion and were averaged. The mean, rather than the maximum, rCBV value was chosen to better reflect the overall degree of vascularity. Areas with necrosis were excluded, as were vascular structures. A Wilcoxon rank-sum test was used to determine whether rCBV values in TDLs and neoplastic lesions were significantly different. A non-parametric test was used because parametric tests are inappropriate with the skewed distributions of rCBV values that were observed in this study.

Results

The diagnosis of tumefactive demyelinating disease was made by surgical biopsy in four patients with special stains for myelin and axons. In the remaining six patients, the diagnosis was made by strong clinical suspicion supported by CSF analysis showing myelin basic protein or oligoclonal bands and/or positive somatosensory evoked potentials. The main criteria of diagnosing TDL in these six patients, however, was clinical follow-up, with or without documented regression of the lesions on images. All patients received IV administered steroid therapy, resulting in marked improvement in their symptoms.

On conventional MR images, all TDLs showed variable but definite contrast enhancement. Most lesions showed peripheral rim enhancement, and one lesion showed solid enhancement (Fig 1A). Le-

sion size varied from 1.0 to 3.5 cm, and all except one was located within the supratentorial cerebral white matter. The one lesion within the posterior fossa was located near the middle cerebellar peduncle. Perilesional signal abnormality on T2-weighted or fluid-attenuated inversion recovery images was also variable, but none showed extensive edema. Moreover, none of the lesions, regardless of size or location, was associated with marked mass effect. Only two of 10 patients had more than one large lesion; one had two lesions, and the other had three. In the patient with three lesions, not all lesions could be included in the dynamic contrast-enhanced MR sections because of the large distance separating the most superior lesion from the most inferior lesion.

For the four patients who underwent stereotactic biopsy, the enhancing portion of the lesion was included in the biopsy specimen. Pathologically, there was extensive demyelination with perivascular inflammatory infiltrates but normal appearing vessels. There were areas of hypercellularity and atypical reactive astrocytes that could have been mistaken for a neoplastic process. Special stains for myelin and axons showed extreme myelin loss, with relative preservation of axonal architecture. There was no evidence of neovascularization in any of the biopsy samples.

For the remaining six patients who did not undergo biopsy, prompt IV administered steroid therapy was begun after MR imaging and resulted in alleviation of symptoms. Five of these patients had either positive CSF results, positive results of their somatosensory evoked potential tests, or both. The remaining patient had equivocal results of his CSF and evoked potential studies. For four of the six patients, follow-up MR imaging or CT studies showed regression of the lesions. One of the two remaining patients subsequently developed a cervical spinal cord lesion that was characteristic of a demyelinating lesion, and the other experienced complete resolution of symptoms.

The control group of patients with intracranial neoplasms were chosen because their conventional MR imaging features were not typical for neoplasms but were similar to those of the TDLs (ie, the tumors had minimal edema and mass effect and well-circumscribed borders). The pathologic diagnoses of the 11 patients were as follows: three glioblastomas multiforme, one anaplastic mixed glioma, two anaplastic astrocytomas, one low-grade oligodendroglioma, and four primary cerebral lymphomas. All tumors were located within the supratentorial compartment and varied in size from 1.0 to 4.5 cm.

Figures 1 (TDL) and 2 (glioblastoma multiforme) show a solidly enhancing, well-circumscribed mass with minimal surrounding edema and no mass effect on conventional MR images. The color overlay of rCBV maps clearly shows increases in vascularity in the glioblastoma multiforme. No increase is seen in the TDL (Fig 1C), however.

Table 1 presents the rCBV values in TDLs and intracranial neoplasms. The rCBV of TDLs ranged from 0.22 to 1.79, with a mean of 0.88 $\pm$ 0.46. The rCBV of neoplasms ranged from 1.55 to 19.20, with a mean of 6.47 $\pm$ 6.52. The Wilcoxon rank-sum test showed that the difference in mean rCBV between the two groups was statistically significant ($P = .009$). Only three (25%) of 12 TDLs had rCBV values >1.0. There was a wide variation in rCBV measurements in the tumor group, whereas all TDLs had rCBV values of <2.0. There were two lymphomas with rCBV <2.0. Table 2 illustrates wide variations in rCBV values among different types of tumors.

The rCBV of lymphomas varied from 1.55 to 2.82, with a mean of 2.11 $\pm$ 0.53. When compared with the mean rCBV of TDLs, the difference was statistically significant ($P = .0053$), albeit not as significant as that between TDLs and high-grade gliomas.

In four patients with TDLs, T2*-weighted echoplanar images acquired during maximum bolus enhancement showed linear ''vessel-like'' structures through the center of the lesion, oriented toward engorged subependymal veins that were not seen on conventional MR images (Fig 3E). These vessel-like structures were only transiently seen during the dynamic phase of injection of contrast agent and were not apparent on either T2-weighted or fluid-attenuated inversion recovery images. When drawing regions of interest for rCBV calculations, care was taken to avoid these possible vessels that could have increased measured rCBV values.

Follow-up information was available for seven of 10 patients. Only one of the seven patients (a 13-year-old female patient) was diagnosed as having classic multiple sclerosis, with subsequent development of a cervical spinal cord lesion. The mean time between the first MR imaging examination and the final clinical follow-up for our 10 patients with TDLs was 9.6 $\pm$ 10.8 months (range, 2–36 months). None of the four patients with biopsy-proved demyelinating disease returned with recurrence of symptoms or MR imaging abnormalities during the follow-up period. This interval may be too short to determine conclusively which patients will go on to develop full-blown multiple sclerosis.

Discussion

This study shows that MR rCBV measurements can be very valuable in differentiating TDLs and intracranial neoplasms that share similar conventional MR imaging features. In addition, the dynamic set of images acquired during bolus injection of contrast agent can provide additional diagnostic clues by showing vascular structures, most likely veins, within the lesion. In this study, these structures were seen only in TDLs.

Despite decades of clinical and experimental research, the exact cause of primary demyelinating

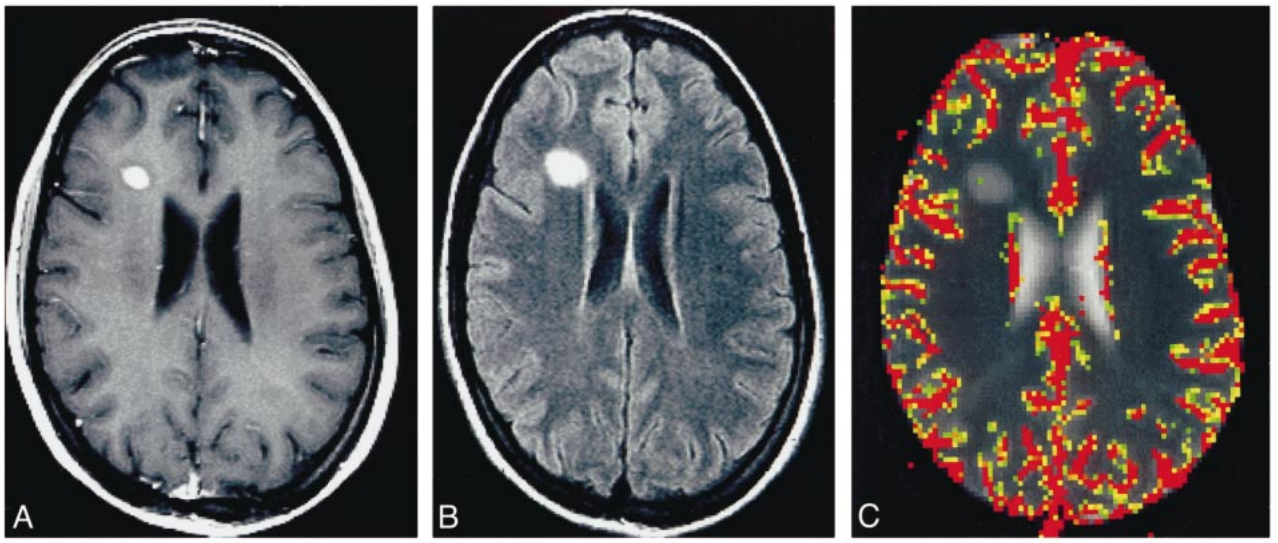

FIG 1. TDL in a 22-year-old woman.
A, Contrast-enhanced T1-weighted image (600/14/1) shows a well-circumscribed solidly enhancing mass in the right frontal lobe.
B, Fluid-attenuated inversion recovery image (9000/110/1) shows a mild degree of signal abnormality around the lesion.
C, Color overlay of rCBV map shows no evidence of increased blood volume.

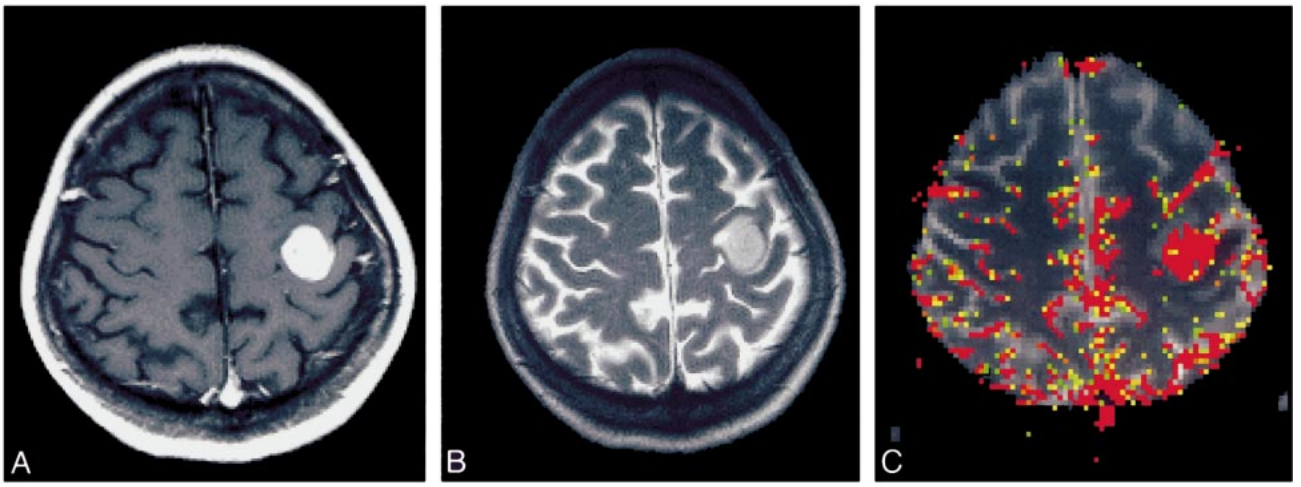

FIG 2. Glioblastoma multiforme in a 63-year-old woman.
A, Contrast-enhanced T1-weighted image (600/14/1) shows a well-circumscribed mass in the left frontal lobe.
B, T2-weighted image (3400/119/1) shows minimal edema and mass effect.
C, Color overlay of rCBV map shows marked increase in blood volume.

TABLE 1: Comparison of rCBV in TDL and intracranial neoplasms

	Range of rCBV	Mean rCBV*	SD
Tumefactive demyelinating lesion (n = 12)	0.22–1.79	0.88	0.46
Intracranial neoplasms (n = 11)	1.55–19.2	6.47	6.52

* $P = .009$

disease of the CNS remains unknown in most cases (4). Multiple sclerosis, the most common and chronic form of demyelinating disease, is characterized classically by a prolonged relapsing-remitting clinical course with multiple periventricular demyelinating plaques (14). There is a subset of patients with demyelinating disease, however, who present with an acute/subacute episode of focal neurologic deficit but do not necessarily develop full-blown multiple sclerosis. It is difficult to determine under which subgroup of demyelinating disorders these patients fall because of highly variable clinical presentations and pathologic findings. On images, the lesions of these patients tend to be solitary, mass-like, and large. It is this type of demyelinating lesion that is frequently mistaken for a neoplasm and may result in surgical biopsy or resection (1, 2, 4–6, 15). Moreover, the pathologic findings may erroneously suggest high-grade tumors, and these patients with TDLs may receive adjuvant radiation therapy after surgery, as if they had anaplastic tumors.

TABLE 2: Pathologic diagnosis and relative cerebral blood volume measurements of patients with intracranial neoplasms

Patient No.	Age (y)	Sex	Pathologic Diagnosis	Maximum Tumor rCBV
1	39	F	Anaplastic mixed glioma	19.2
2	63	F	Glioblastoma	18.7
3	51	M	Anaplastic astrocytoma	8.7
4	70	M	Glioblastoma	5.8
5	70	M	Glioblastoma	3.23
6	28	F	Oligodendroglioma	2.27
7	29	F	Anaplastic astrocytoma	4.87
8	54	M	Primary cerebral lymphoma	2.14
9	51	M	Primary cerebral lymphoma	1.55
10	51	M	Primary cerebral lymphoma	2.82
11	37	M	Primary cerebral lymphoma	1.94

A review of the literature on tumefactive demyelinating disease reiterates the dilemma in diagnosis and classification of large demyelinating lesions (1–3, 5, 7, 16, 17). It is not clear when the word *tumefactive* was first used in the literature to describe large dominant ''tumor-like'' demyelinating lesions that are frequently misdiagnosed as brain tumors. It is also uncertain how many of these patients go on to develop clinical diagnosis of definite multiple sclerosis. Although some of these lesions were originally categorized as lesions of multiple sclerosis, further analysis supported by long-term clinical follow-up has shown that these lesions may represent a distinct clinical entity from classic multiple sclerosis. In a review of 31 patients presenting with large focal demyelinating lesions, Kepes (5), in 1993, found that most of these patients had each experienced a single acute attack as a rule rather than as an exception and suggested a separate entity intermediate between classic multiple sclerosis and acute disseminated encephalomyelitis. Dagher and Smirniotopoulos (17) reviewed conventional CT and MR imaging findings of 21 cases of pathologically confirmed tumefactive demyelinating disease. They suggested that these lesions represent an ill-defined subgroup of demyelinating disease with atypical clinical presentation and imaging findings (ie, few lesions with prominent edema and mass effect located in an atypical location).

The diagnostic challenge in differentiating large dominant TDLs from high-grade gliomas or other intracranial neoplasms, both radiologically and pathologically, is well known (1, 2, 5, 6, 15, 16). When there are multiple periventricular white matter lesions in the appropriate clinical setting, the diagnosis of demyelinating disease is straightforward. Involvement of the major white matter tracts, such as the corpus callosum and/or the brachium pontis, and the presence of additional lesions in the dorsolateral aspect of the spinal cord also support the diagnosis of demyelinating disease. In addition, the presence of optic neuritis with white matter lesions is highly suggestive of demyelinating disease rather than neoplasms. When the lesion is a solitary dominant mass without typical white matter abnormalities of demyelination and clinical presentation suggests a space-occupying mass lesion, an intracranial neoplasm cannot be excluded with confidence. The diagnostic difficulty in differentiating TDLs from brain tumors is not limited to imaging. On pathologic evaluation, TDLs can be mistakenly diagnosed as high-grade gliomas. Five specific pathologic patterns are common to demyelinating lesions and high-grade glial neoplasms: hypercellularity; pleomorphic reactive astrocytes with large, hyperchromatic nuclei; mitotic figures; presence of necrotic areas; and areas of cystic degeneration or cavitation (1). Despite some similar histopathologic features, TDLs and high-grade neoplasms are different regarding vascularity. Although vascular changes have been reported in TDLs, including enlargement of endothelial cells, florid angiogenesis is distinctly absent (18). A previous study has shown similar vascular changes in TDLs with vascular hyperplasia (ie, increased number of vascular cell layers without formation of neocapillaries), seen in only one of 17 specimens (1). Again, frank neovascularization is absent in TDLs. High-grade gliomas, on the other hand, are characterized and graded by the presence and degree of tumor angiogenesis (11). Despite lack of true angiogenesis, TDLs can still be mistaken for high-grade gliomas, usually anaplastic astrocytomas, because of features such as astrocyte pleomorphism, necrosis, and mitotic figures, or oligodendrogliomas, due to activated histiocytes simulating round tumor nuclei with perinuclear halos (19). For our four patients who underwent surgical diagnosis, none of the biopsy specimens showed evidence of neovascularization. All specimens were subjected to special stains for myelin and axons, which allowed accurate diagnosis of demyelinating disease.

The differential diagnosis between TDLs and high-grade tumors can also be challenging using imaging studies. Conventional MR imaging features of TDLs and high-grade neoplasms can be very similar: both can enhance, may contain areas of necrosis/cystic degeneration, and tend to occur within the cerebral white matter. Contrast enhancement on MR images reflects underlying blood-brain barrier breakdown and is a nonspecific finding that occurs in many different intracranial disease processes, including but not limited to tumors, infection, inflammation, and certain stages of infarction and hemorrhage. Enhancement in TDLs is thought to correlate with the degree of macrophage infiltration and related blood-brain barrier breakdown, which is a relatively early histologic finding in cases of acute lesions (6). Contrast enhancement of intracranial neoplasms, high-grade tumors in particular, is common because of blood-brain barrier breakdown in preexisting vessels and newly formed tumor capillaries that lack blood-brain barrier. Conversely, some highly anaplastic gliomas may not enhance at all (20, 21). Therefore, lack of specific-

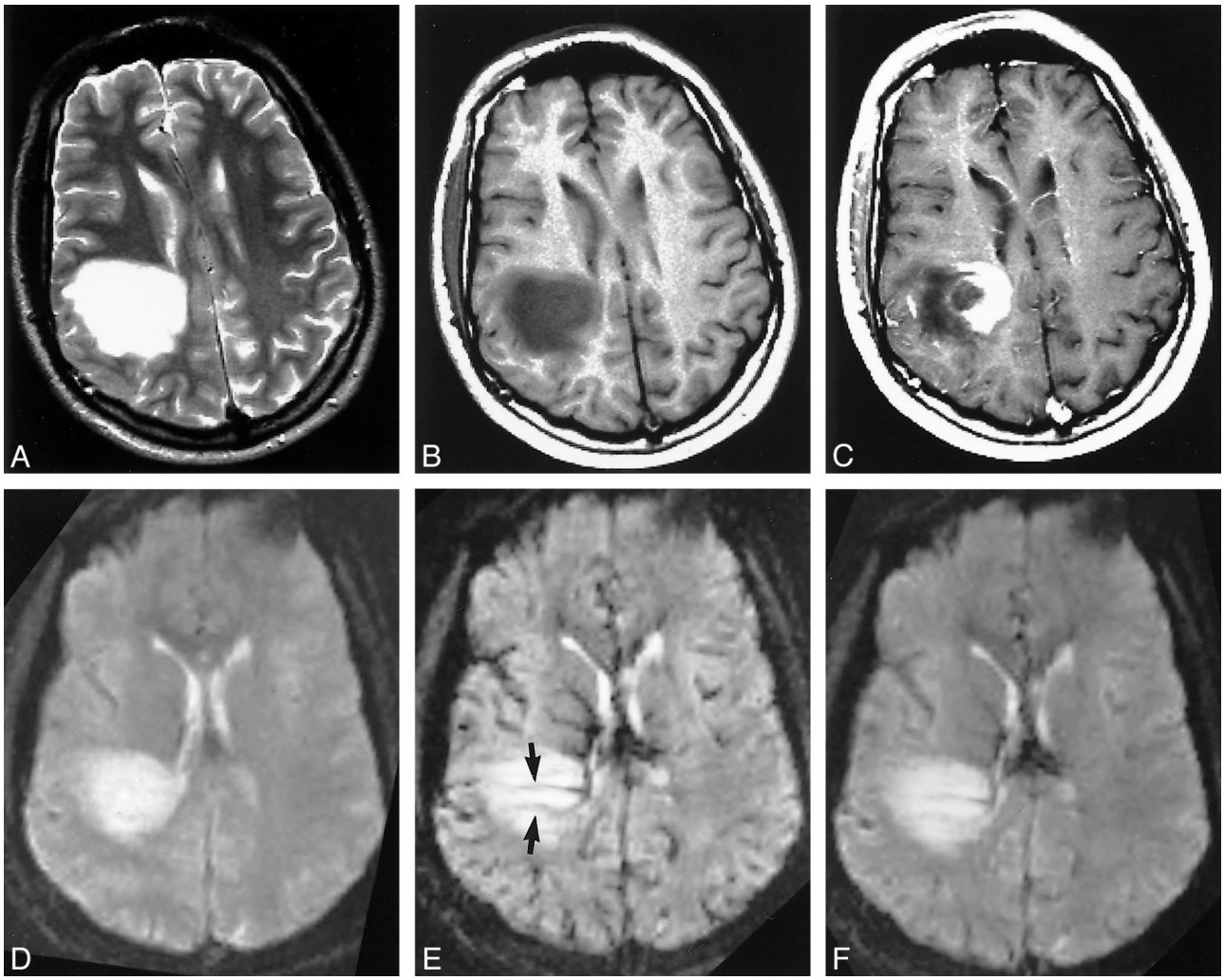

FIG 3. TDL in a 37-year-old man.

A, T2-weighted image (3400/119/1) shows a large hyperintense mass lesion in the right parietal lobe. There are no visible flow voids within the lesion.

B, Unenhanced T1-weighted image (600/14/1) shows hypointense signal of the lesion.

C, Contrast-enhanced T1-weighted image (600/14/1) shows heterogeneous enhancement of the medial aspect of the lesion in a concentric pattern.

D, Dynamic T2*-weighted image (1000/54/1) obtained before IV administration of contrast agent.

E, Dynamic T2*-weighted image (1000/54/1) obtained during IV administration of contrast agent shows several periventricular, linear vessel-like structures (*arrows*) running through the center of the lesion near a dilated subependymal vein. The dominant lesion itself shows no signal loss.

F, Dynamic T2*-weighted image (1000/54/1) obtained 50 s after IV administration of contrast agent shows return of brain signal to baseline, with residual signal loss within the aforementioned linear vessel-like structures.

ity of contrast enhancement renders it ineffective in differentiating TDLs from high-grade gliomas. In addition, presence of necrosis/cystic degeneration on MR images can be seen in both high-grade gliomas, such as glioblastomas multiforme, and in TDLs.

Dynamic contrast-enhanced T2*-weighted MR imaging allows measurements of cerebral blood volume that complement the anatomic information provided by conventional MR imaging. With a combined imaging and processing time of <3 minutes, using a standard dose of contrast agent, dynamic contrast-enhanced MR imaging provides fast and reliable information on lesion vascularity that matches catheter angiography without added risk. It has become a valuable diagnostic tool in the evaluation of intracranial neoplasms and has been useful in grading glial tumors, guiding stereotactic biopsy, and monitoring treatment response to antiangiogenic agents such as thalidomide (12, 22, 23). Our study shows that MR rCBV measurements reveal diagnostically useful differences between TDLs and high-grade glial neoplasms. The difference in rCBV values between TDLs and lymphomas was less pronounced, but the mean rCBV values were significantly different between the two entities. All lymphomas had rCBV values >1.5, whereas only one of 12 TDLs had rCBV values >1.5. When comparing TDLs and lymphomas, however, conventional MR imaging features were

more valuable in differentiating the two. All lymphomas showed iso- or hypointense signal abnormality compared with the adjacent brain on T2-weighted images, whereas all TDLs showed hyperintense signal abnormality. In addition, lymphomas showed more prominent perilesional edema than did TDLs. Dynamic contrast-enhanced T2*-weighted imaging along with conventional MR imaging may enable a correct diagnosis when considered in conjunction with both clinical and laboratory evaluations and may obviate unnecessary surgery and allow the prompt initiation of appropriate medical treatment. Our results suggest that when dynamic contrast-enhanced T2*-weighted MR imaging features are taken into consideration along with conventional MR imaging and clinical/laboratory findings, TDLs and intracranial tumors can be differentiated with high level of confidence.

Aronen et al (22) reported rCBV measurements of high-grade gliomas of <2.0, whereas in our study, the rCBV measurements of all the high-grade gliomas were >2.0. It is difficult to conclude why there is such a difference. It may be, in part, because of the difference in patient populations. On the other hand, there are several technical differences that might explain the discrepancy. First, Aronen et al used double dose contrast and spin-echo echo-planar imaging whereas we used single dose and gradient-echo echo-planar imaging. Another difference is in the method used to correct for contrast agent leakage; we used baseline subtraction, whereas Aronen et al used gamma variate fitting. The differences in fitting algorithm may be a factor in the differences in rCBV calculation.

Perivenular demyelination is one of the classical and the most specific pathologic features of idiopathic primary demyelinating diseases of the CNS (4, 24). In other white matter diseases of the CNS in which selective myelin destruction occurs, such as the inherited leukodystrophies, progressive multifocal leukoencephalopathy, central pontine myelinolysis, and other toxic/hypoxic leukoencephalopathies, there is distinct absence of perivenular myelin involvement (4, 25). Recently, Tan et al (26) showed the perivenular distribution of demyelinating plaques in the brain using 3D gradient-echo MR venography. Our dynamic T2*-weighted images show similar venous anatomy that is characteristic of primary demyelinating disease of the brain. In four of 12 TDLs and in none of our patients with tumors, we observed linear structures running through the center of the lesion. These linear structures were best seen at the moment of greatest signal intensity drop during the dynamic acquisition (Fig 3E). Although there is no direct histopathologic correlation, we think that these are veins or venules that join the subependymal veins along the lateral ventricular margin and that are surrounded by areas of demyelination. This seems likely for three reasons. First, these structures are anatomically similar in shape and location for periventricular veins. Second, they appear to connect with or ''drain into'' adjacent subependymal veins. Third, they are transiently seen during the dynamic phase of echo-planar imaging, as one would expect for a vascular structure.

Figure 3E shows not only the veins within the area of demyelination but also the engorgement of the adjacent subependymal veins, indicative of venous hyperemia, probably related to inflammatory response to demyelination around the deep draining veins. It is possible that our cases of TDLs represent exacerbation of an acute demyelinating process occurring around perivenular structures that may lead to the MR imaging findings mentioned above.

Conclusion

By serving as a measure of lesion vascularity, dynamic contrast-enhanced T2*-weighted MR imaging can be valuable in differentiating TDLs from intracranial neoplasms. A combination of strong clinical suspicion with characteristic dynamic contrast-enhanced T2*-weighted MR imaging features may lead to correct diagnosis of demyelinating lesions and may obviate any invasive surgical intervention.

References

1. Zagzag D, Miller DC, Kleinman GM, Abati A, Donnenfeld H, Budzilovich GN. **Demyelinating disease versus tumor in surgical neuropathology: clues to a correct pathological diagnosis.** *Am J Surg Pathol* 1993;17:537–545
2. Hunter SB, Ballinger WE Jr, Rubin JJ. **Multiple sclerosis mimicking primary brain tumor.** *Arch Pathol Lab Med* 1987;111: 464–468
3. Giang DW, Poduri KR, Eskin TA, et al. **Multiple sclerosis masquerading as a mass lesion.** *Neuroradiology* 1992;34:150–154
4. Prineas JW, McDonald WI. **Demyelinating diseases.** *Greenfield's Neuropathology.* ed 6. vol I. New York: Wiley; 1997:814–846
5. Kepes JJ. **Large focal tumor-like demyelinating lesions of the brain: intermediate entity between multiple sclerosis and acute disseminated encephalomyelitis? a study of 31 patients.** *Ann Neurol* 1993;33:18–27
6. Nesbit GM, Forbes GS, Scheithauer BW, Okazaki H, Rodriguez M. **Multiple sclerosis: histopathologic and MR and/or CT correlation in 37 cases at biopsy and three cases at autopsy.** *Radiology* 1991;180:467–474
7. Kurihara N, Takahashi S, Furuta A, et al. **MR imaging of multiple sclerosis simulating brain tumor.** *Clin Imaging* 1996;20: 171–177
8. Burger PC, Vogel FS. **The brain: tumors.** In: Burger PC, Vogel FS, eds. *Surgical Pathology of the Central Nervous System and Its Coverings.* New York: Wiley; 1982:223–266
9. Burger PC, Vogel FS, Green SB, Strike TA. **Glioblastoma multiforme and anaplastic astrocytoma: pathologic criteria and prognostic implications.** *Cancer* 1985;56:1106–1111
10. Burger P. **Malignant astrocytic neoplasms: classification, pathology, anatomy, and response to therapy.** *Semin Oncol* 1986; 13:16–20
11. Daumas-Duport C, Scheithauer B, O'Fallon J, Kelly P. **Grading of astrocytomas: a simple and reproducible method.** *Cancer* 1988;62:2152–2165
12. Knopp EA, Cha S, Johnson G, et al. **Glial neoplasms: dynamic contrast-enhanced T2*-weighted MR imaging.** *Radiology* 1999; 211:791–798
13. Cha S, Lu S, Johnson G, Knopp EA. **Dynamic susceptibility contrast MR imaging: correlation of signal intensity changes with cerebral blood volume measurements.** *J Magn Reson Imaging* 2000;11:114–119

14. Poser CM, Paty DW, Scheinberg L, et al. **New diagnostic criteria for multiple sclerosis: guidelines for research protocols.** *Ann Neurol* 1983;13:227–231
15. Rieth KG, Di Chiro G, Cromwell LD, et al. **Primary demyelinating disease simulating glioma of the corpus callosum: report of three cases.** *J Neurosurg* 1981;55:620–624
16. Kalyan-Raman UP, Garwacki DJ, Elwood PW. **Demyelinating disease of corpus callosum presenting as glioma on magnetic resonance scan: a case documented with pathological findings.** *Neurosurgery* 1987;21:247–250
17. Dagher AP, Smirniotopoulos J. **Tumefactive demyelinating lesions.** *Neuroradiology* 1996;38:560–565
18. Charcot JM. **Histologie de la sclerose en plaques.** *Gaz Hop* 1868; 41:554–566
19. Lantos PL, Vandenberg SR, Kleihues P. **Tumours of the nervous system.** *Greenfield's Neuropathology.* ed 6. vol II. New York: Wiley; 1997:635
20. Ginsberg LE, Fuller GN, Hashmi M, Leeds NE, Schomer DF. **The significance of lack of MR contrast enhancement of supratentorial brain tumors in adults: histopathological evaluation of a series.** *Surg Neurol* 1998;49:436–440
21. Barker FG, Chang SM, Huhn SL, et al. **Age and the risk of anaplasia in magnetic resonance-nonenhancing supratentorial cerebral tumors.** *Cancer* 1997;80:936–941
22. Aronen HJ, Gazit IE, Louis DN, et al. **Cerebral blood volume maps of gliomas: comparison with tumor grade and histologic findings.** *Radiology* 1994;191:41–51
23. Cha S, Knopp EA, Johnson G, et al. **Dynamic contrast-enhanced T2-weighted MR imaging of recurrent malignant gliomas treated with thalidomide and carboplatin.** *AJNR Am J Neuroradiol* 2000;21:881–890
24. Adams C. **Vascular aspects of multiple sclerosis.** *A Colour Atlas of Multiple Sclerosis & Other Myelin Disorders.* London: Wolfe Medical Publications; 1989:184–187
25. Adams RD. **A comparison of the morphology of the human demyelinating diseases and experimental "allergic" encephalomyelitis.** In: Kies MW, Alvord EC, eds. *"Allergic" Encephalomyelitis.* Springfield: Charles C Thomas; 1959:183–209
26. Tan IL, van Schijndel RA, Pouwels PJ, et al. **MR venography of multiple sclerosis.** *AJNR Am J Neuroradiol* 2000;21:1039–1042